Available online at www.sciencedirect.com

ScienceDirect

Palaeoworld 28 (2019) 429–440

Palaeoworld

www.elsevier.com/locate/palwor

Middle Triassic conodont apparatus architecture revealed by synchrotron X-ray microtomography

Jin-Yuan Huang [a,b,c,d,*], Carlos Martínez-Pérez [b,e], Shi-Xue Hu [a], Philip C.J. Donoghue [e], Qi-Yue Zhang [a], Chang-Yong Zhou [a], Wen Wen [a], Michael J. Benton [e], Mao Luo [f], Hua-Zhou Yao [g], Ke-Xin Zhang [c]

[a] *Chengdu Center of China Geological Survey, Chengdu 610081, China*
[b] *Cavanilles Institute of Biodiversity and Evolutionary Biology, University of Valencia, C/Catedràtic José Beltrán Martínez, 2, 46980 Paterna, Valencia, Spain*
[c] *Institute of Geological Survey, China University of Geosciences (Wuhan), Wuhan 430074, China*
[d] *State Key Laboratory of Palaeobiology and Stratigraphy, Nanjing Institute of Geology and Palaeontology, Chinese Academy of Sciences, Nanjing 210008, China*
[e] *School of Earth Sciences, University of Bristol, Life Sciences Building, Tyndall Avenue, Bristol, BS8 1TQ, UK*
[f] *Deakin University, Geelong, School of Life and Environmental Sciences (Burwood Campus), 221 Burwood Highway, Burwood, Victoria 3125, Australia*
[g] *Wuhan Center of China Geological Survey, Wuhan 430205, China*

Received 7 March 2018; received in revised form 14 July 2018; accepted 16 August 2018
Available online 23 August 2018

Abstract

The composition of conodont apparatuses is crucial for understanding the feeding mechanisms of these early vertebrates. However, the multi-element apparatus reconstructions of most species remain equivocal because they have been inferred from loose element collections, guided by knowledge from rare articulated 'bedding plane assemblages' and fused clusters, often from distantly related taxa. Even these natural assemblages can be difficult to interpret because the component elements can be closely juxtaposed or embedded in matrix, making it hard to discern the morphology of each element and their relative positions within the architecture of the feeding apparatus. Here we report five exceptionally preserved conodont clusters from the Middle Triassic Luoping Biota, Yunnan Province, Southwest China. These materials were scanned using synchrotron radiation X-ray tomographic microscopy (SRXTM), revealing the morphology and positional homology of the component elements in the fused clusters. We confirm that the apparatus of *Nicoraella* was composed of eight types of elements, comprising a total of 15 elements. SRXTM reveals the positional homologies of the component elements, viz. a single alate element is located in the S_0 position, flanked successively abaxially by pairs of breviform digyrate S_1 and S_2 elements, bipennate S_3 and S_4 elements, and a pair of inwardly curved breviform digyrate M elements. Carminate elements occupy the P_1 and P_2 positions. The apparatus of *Nicoraella* is among the most completely characterised of all conodonts and serves as a template for the reconstruction of gondollellids.

Keywords: Fused conodont clusters; 15-element apparatus; Anisian; Luoping Biota; Southwest China

1. Introduction

Conodonts are an extinct clade of jawless vertebrates (e.g., Donoghue et al., 2000), which occur abundantly in carbonate deposits from the upper Cambrian to the latest Triassic. Their tooth-like skeletal elements (oral denticles) have been widely used for biostratigraphic correlation (e.g., Jiang et al., 2007, 2011), inferring evolutionary patterns (e.g., Chen et al., 2016) and palaeoenvironmental interpretation (e.g., Chen et al., 2015). Conodont apatite is also an important archive of seawater chem-

* Corresponding author at: Chengdu Center of China Geological Survey, Chengdu 610081, China.
E-mail addresses: hjinyuan@cgs.cn (J.Y. Huang), carlos.martinez-perez@uv.es (C. Martínez-Pérez), hushixue@126.com (S.X. Hu), phil.donoghue@bristol.ac.uk (P.C.J. Donoghue), yxzqy@sina.com (Q.Y. Zhang), zhcy79@163.com (C.Y. Zhou), wenwen2020240@163.com (W. Wen), mike.benton@bristol.ac.uk (M.J. Benton), maoluo@nigpas.ac.cn (M. Luo), ycxc2009@126.com (H.Z. Yao), kx_zhang@cug.edu.cn (K.X. Zhang).

https://doi.org/10.1016/j.palwor.2018.08.003
1871-174X/

istry exploited in particular, to infer sea temperature through the Palaeozoic (e.g., Joachimski et al., 2012; Sun et al., 2012).

As ancient jawless vertebrates, the feeding mechanisms of conodonts, as reflected in the anatomy and architecture of their feeding apparatuses, have attracted considerable attention. Although several apparatus models have been reconstructed for different conodont species based on discrete elements, fused clusters, bedding plane assemblages and articulated assemblages associated with the soft-tissues of conodonts (Purnell and Donoghue, 1997, 1998; Orchard, 2005; Goudemand et al., 2011, 2012; Agematsu et al., 2017; Zhang et al., 2017), discrepancies remain among these models. In large part, this is because even in natural assemblages (bedding plane assemblages and fused clusters) the component elements are obscured by one another and/or the surrounding matrix. In this context, the application of non-destructive tomographic techniques can provide new opportunities to study conodont apparatus architecture, especially in the case of fused cluster natural assemblages, which have been under-utilised in attempts to reconstruct the architecture of conodont feeding apparatuses since the elements are so closely juxtaposed and obscured by diagenetic mineral crusts.

In order to demonstrate the potential of tomographic techniques for resolving conodont apparatus architecture, we describe five exceptionally preserved fused conodont clusters of *Nicoraella* from the Middle Triassic Luoping Biota, Yunnan Province, Southwest China. These clusters were characterised tomographically using synchrotron radiation X-ray tomographic microscopy (SRXTM) to resolve their morphology and apparatus composition. Our results allow us to test the reliability of previous reconstructions based on the same material using traditional SEM studies (Huang et al., 2019), and establish constraints on hypotheses on the functional kinematics of conodont feeding apparatuses.

2. Previous applications of synchrotron tomography in conodont palaeobiology

The introduction of novel techniques of high resolution computed tomography has opened new opportunities in palaeobiology, and conodont clusters have been a focus of new palaeobiological and functional studies. From their first application, tomographic techniques have been demonstrated to have great potential, not only for apparatus reconstruction, but also for unravelling the function, development and evolution of conodont skeletal tissues. Several studies have used synchrotron-derived data to apply computational biomechanical techniques, including Finite Element Analysis, to inform debate over conodont element function. Several conodont groups have been studied, including the simple cone-shaped elements of *Panderodus* (Murdock et al., 2013a, 2014), the carminate P elements of *Wurmiella* (Jones et al., 2012a, 2012b), platform P_1 elements of ozarkodinid conodonts including *Gnathodus*, *Polygnathus*, and *Pseudofurnishius* (Martínez-Pérez et al., 2014a, 2014b, 2016), and the icriodontid *Caudicriodus woschmidti* (Suttner et al., 2017). These studies have demonstrated that conodont elements performed a tooth-like function and that occlusal kinematics of conodonts are as disparate as their element morphologies.

The application of synchrotron tomography has also informed understanding of the evolution of conodont skeletal tissues and the phylogenetic affinity of conodonts. Murdock et al. (2013b) demonstrated the stepwise acquisition of euconodont characters from paraconodonts, rejecting the homology of euconodont crown tissue and vertebrate enamel, and demonstrating that these tissues evolved independently and convergently. More recent work has focused on the ontogeny of conodont elements, revealing the evolutionary processes that affected conodonts through their growth (Mazza and Martínez-Pérez, 2015, 2016). These studies also showed that the ontogenetic growth record of conodont elements can be used to discriminate homology from homoplasy. Evidently, synchrotron tomography is a powerful tool for investigating conodont ontogeny, ecology, evolution and phylogenetic relationships.

Finally, some synchrotron-based conodont analyses have focused on apparatus reconstruction. Goudemand et al. (2011) were the first to reconstruct a conodont apparatus using synchrotron tomography, based on a partial cluster of *Novispathodus* from the lowermost Spathian of the Tsoteng section (Tiandong County, Guangxi, China). Later, Goudemand et al. (2012), adding new material, confirmed previous *Novispathodus* apparatus reconstructions, but revised homology of the $S_{1–4}$ ramiform elements. Two key studies have attempted to reconstruct the apparatus of the earliest Triassic *Hindeodus parvus*. Agematsu et al. (2017), based on bedding plane assemblages from Japan, confirmed a 15-element apparatus, whereas Zhang et al. (2017), based on six partial clusters of *Hindeodus parvus* from the Shangsi section (Lower Triassic, Sichuan Province, Southwest China), suggest that the taxa reduced their dentition through phylogeny, eliminating the P_2 element position (but see Agematsu et al., 2018 and Purnell et al., 2018). Finally, Suttner et al. (2017) described a cluster of the icriodontid *Caudicriodus woschmidti* from the Lower Devonian of Austria, showing an apparatus composed of one pair of icriodontan (I) elements and ten pairs of coniform (C1–5) elements.

3. Geological setting and the study section

Triassic deposits, represented mainly by the Feixianguan, Jialingjiang, Guanling, Yangliujing, Zhuganpo, and Xiaowa formations, outcrop widely in western Guizhou and eastern Yunnan Province, Southwest China (Enos et al., 2006). Exceptionally preserved Triassic fossil lagerstätten, such as the Luoping Biota, Panxian Fauna, Xingyi Fauna, and Guanling Biota are located in these areas. Among them, the Luoping Biota has been interpreted to represent a fully recovered shallow marine ecosystem after the end-Permian Mass Extinction (Chen and Benton, 2012; Benton et al., 2013). This biota is preserved in Member II of the Guanling Formation, which consists of nodular limestones, silty limestones, micritic limestones, and bands of dolomite, while Member I of the Guanling Formation consists mainly of mudstones and argillaceous dolomites with a volcanic ash bed (green pisolite) (Zhang et al., 2009).

Three quarries have been excavated to study the abundant fossil materials of the Luoping Biota, named Shangshikan, Menqianpo, and Xiangdongpo, respectively (Zhang et al., 2009;

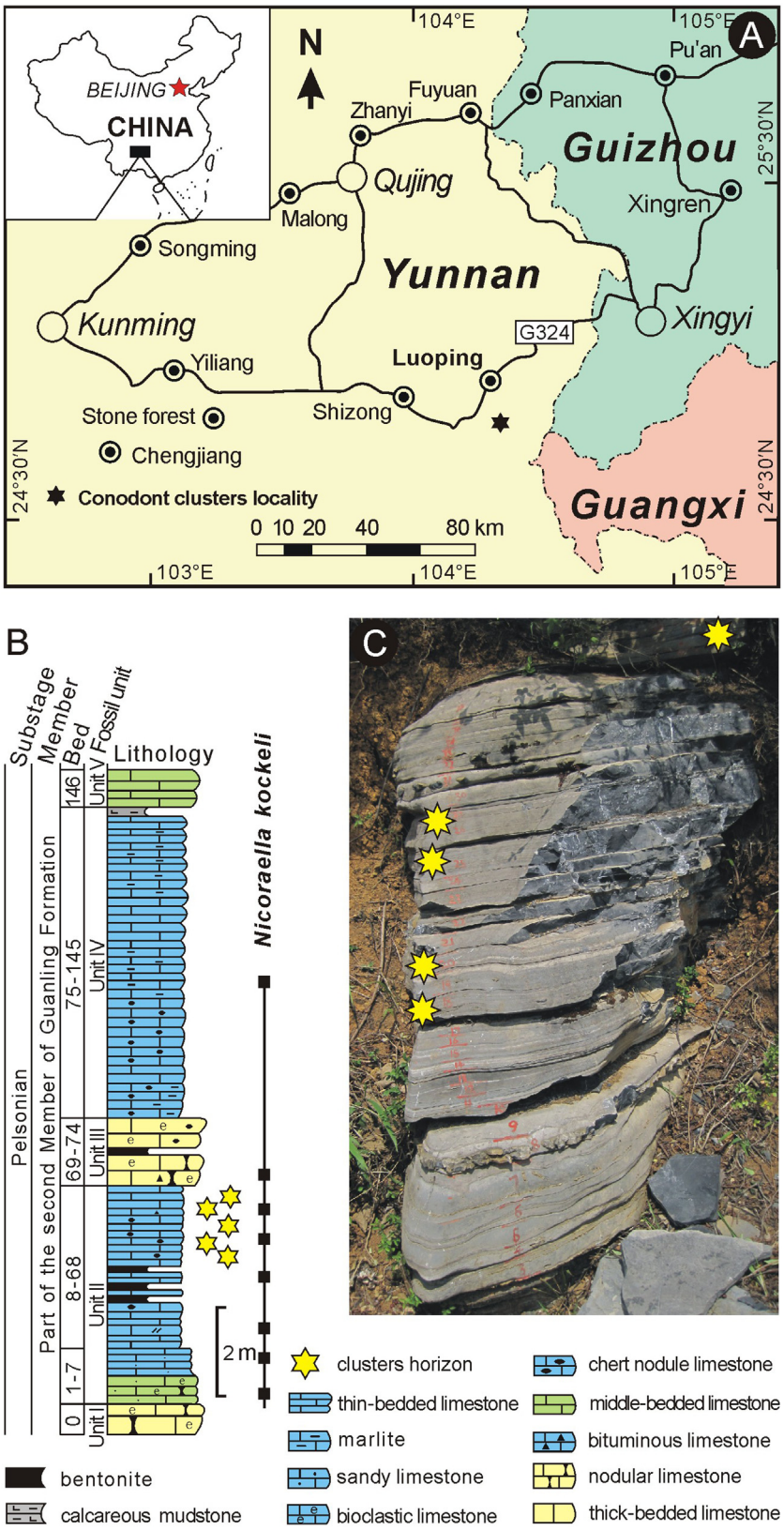

Fig. 1. Location map of the Dawazi section in Luoping County, eastern Yunnan Province, Southwest China (A). The conodont clusters horizons in the Dawazi section (B) and their corresponding layers of the outcrops (C).

Bai et al., 2011; Hu et al., 2011; Luo et al., 2017, 2019). The Dawazi section (24°46′08″N, 104°18′48″E) is a naturally exposed succession, located near the Menqianpo quarry in Dawazi village, about 15 km south of Luoping County (Fig. 1). This section includes all of the fossil-bearing horizons of the Luoping Biota, mainly consisting of carbonate rocks, about 40 m thick, with a slight SE strike and 10° dip, interpreted as an inter-platform basin (Bai et al., 2011). Five units could be identified in the Dawazi section (Huang et al., 2011). Of these, Unit I (Bed 0), Unit III (Beds 69–74) and Unit V (Beds 146–167) are composed mainly of grey medium- to thick-bedded limestone and dolomitic limestone rocks with abundant bioclastics. Unit II (Beds 1–68) and Unit IV (Beds 75–145) are the fossil-bearing horizons of the Luoping Biota, composed of black laminated-bedded micrites intercalated with black siliceous concretions. Many exceptionally preserved marine vertebrates and invertebrates have been collected from these two units, including marine reptiles, fishes, and lightly sclerotized arthropods, associated with bivalves, gastropods, ammonoids, brachiopods, belemnoids, echinoderms, horseshoe crabs, cycloids, foraminifers, ostracods, conodonts, and trace fossils (Hu et al., 2011, 2017; Feldmann et al., 2012, 2017; Wen et al., 2012, 2013; Huang et al., 2013; Liu et al., 2017; Luo et al., 2017, 2019).

Conodonts are abundantly preserved in the section, but the fused clusters have been recovered mainly from Unit II (Fig. 1B, C) (see Huang et al., 2019 for a detailed description of the clusters recovered from this section). The presence of the index conodont *Nicoraella kockeli* suggests that the Luoping Biota is Pelsonian, Anisian, Middle Triassic in age (Huang et al., 2009; Zhang et al., 2009).

4. Materials and methods

Five fused conodont clusters were all collected from the Dawazi section. In particular, two clusters are highly compressed together without much intervening diagenetic mineral, and one of them represents a complete apparatus of 15 elements. The other three clusters appear to preserve aspects of their original three-dimensional arrangement. All the clusters were recovered from heavy liquid density-separation of the residues from acid-digested limestones (Jiang et al., 2004). In order to interpret the pattern of elements in the apparatus, these clusters were scanned using SRXTM at the X02DA TOMCAT beamline of the Swiss Light Source, Paul Scherrer Institute (Villigen, Switzerland). The specimens were scanned using a 20× objective, with exposure time between 180 to 200 ms at 13–17 keV, acquiring 1501 projections equiangularly over 180°. Projections were post-processed and rearranged into flat- and dark-field-corrected sinograms, and reconstruction was performed on a 60-core Linux PC farm using a Fourier transform routine and a regridding procedure (Marone et al. 2010). The resulting volume has isotropic voxel dimensions of 0.325 μm. Slice data were interpreted and manipulated using the software Avizo 8 to extract the digital elements of the apparatus, at the University of Bristol. Virtual models were manipulated using the software Geomagic Studio ver. 12 (Geomagic, Rock Hill, SC, USA). All fused clusters are housed at the Chengdu Center of China Geological Survey, China.

Our description of the clusters relies upon prior knowledge of the biological axes which were inferred from the relative arrangement of the apparatus within the species and specimens that preserve associated soft tissue remains from which these axes can be observed directly (Aldridge et al., 1993, 1995; Purnell et al., 2000). Thus, we infer the cusps of elements in the S_0 and M positions occupy a rostrad position within the apparatus, and P_1 elements occupy the most caudad position; the anterior-posterior axis of P_1 and P_2 elements is aligned ventrally-dorsally, respectively; the cusps of the $S_{1–4}$ elements occupy a ventral position within the apparatus, while their posterior processes occupy a more dorsal position (Purnell et al., 2000).

5. Results and discussion

Our data demonstrate that the apparatus of *Nicoraella* comprises 15 elements, with approximately symmetrical pairs of elements in the S_1, S_2, S_3, S_4, M, P_1, and P_2 positions, and a single alate element located in the S_0 position on the median plane, confirming previous proposals based on SEM analysis of the extensive cluster collection recovered from the same levels (Huang et al., 2019). Element morphologies, relative locations and arrangement, are described below (Sections 5.1 and 5.2).

5.1. *Conodont clusters of* Nicoraella

Two clusters are completely exposed without obscuring encrusting mineral (Figs. 2 and 3). One cluster (pm028-20-wy1-C3; Fig. 2) is highly compressed, and composed of ten elements. One broken breviform digyrate element adheres to the rostral portion of the S array, and is easily diagnosed by the two pairs of hindeodellan elements overlapping the enantiognathiform element in dextral and sinistral views (Fig. 2A, B). The anterior of two S_1 elements are clearly observed in sinistral view. The short inner lateral processes of the enantiognathiform elements can be observed from the ventral side. The S_0 element is recognizable from an oblique ventro-sinistral perspective, with two short lateral processes.

The second cluster (pm028-18-wy1-C1; Fig. 3) is the most completely preserved. It includes all 15 elements of the apparatus, like other ozarkodinid apparatuses, namely nine S elements, two M elements, two P_1 elements, and two P_2 elements, with the opposing M elements flanking the ramiform S elements (Fig. 3). The ventral surfaces of the S_2–S_4 elements are parallel to each other in dextral and sinistral views. The S_1 elements are sandwiched between the two lateral processes of the S_2 elements. A single S_0 element is located in the innermost part of the cluster, and it is oriented at an oblique angle to all of the other S elements (Figs. 3–6). The dextral and sinistral denticles of the P_1 and P_2 elements are occluded, and they are fused to the S elements, connected by the only remaining process of the dextral M element. All denticles are partially broken, as shown in Fig. 3.

Three clusters are partly enveloped within the matrix (Figs. 4–6), preserving aspects of the original three-dimensional

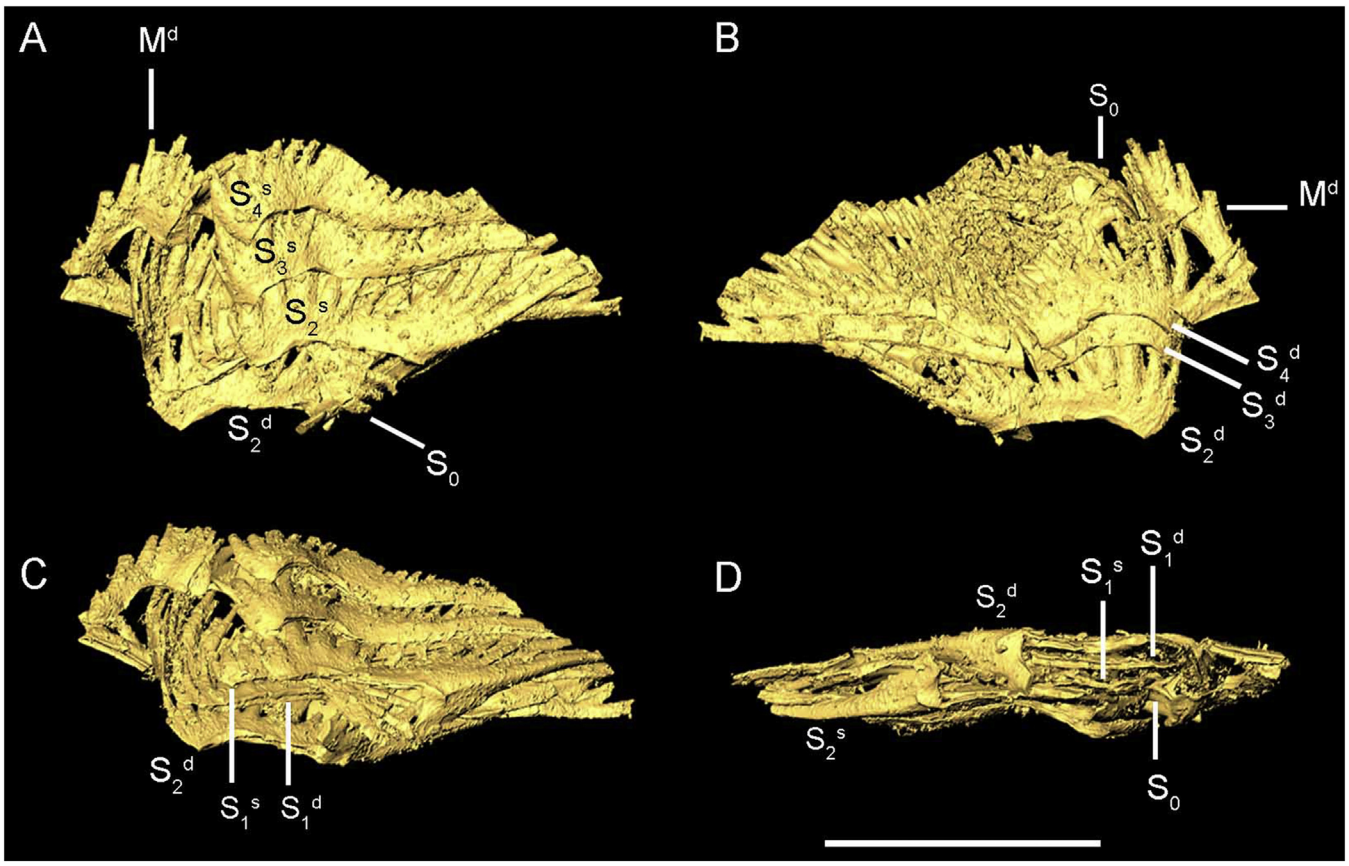

Fig. 2. Articulated conodont clusters from bed 20 in the Dawazi section (catalogue no. pm028-20-wy1-C3). All figures are scanned by synchrotron, from the sinistral (A), dextral (B), ventro-dextral with slightly oral (C), and ventral sides (D) respectively. Scale bar = 400 μm.

arrangement of the elements. One cluster (pm028-25-wy1-C1; Fig. 4) is composed of 13 elements, but most parts of the S elements are hidden in the matrix. The rostrad sides of the posterior processes of two M elements are exposed, but their cusps and lateral processes are lost. The S_0 element is fully enclosed in the matrix, and only the two lateral processes are exposed. Two prominent, long-cusped P_2 elements are fused together with the S array. The dextral and sinistral divisions of the S-M domains exhibit approximately bilateral symmetry in oral, ventral and dorsal views, but the sinistral and dextral S arrays are displaced along the rostro-caudal axis.

A fourth cluster (pm028-25-wy1-C2; Fig. 5) is composed of 11 elements, of which two M elements and the sinistral S elements can be discerned, while the dextral S elements remain concealed by the matrix. Two denticles are preserved on the inner lateral process of the S_2 elements. The M elements appear to have settled on the same plane in sinistral view. All sinistral S-M elements occur caudad of their dextral counterparts, but the bilateral arrangement of the S elements is evident from the ventral side.

The fifth cluster (pm028-26-wy1-C1; Fig. 6) is composed of ten elements; all S and M elements are fused together by intervening matrix. The surface of the cluster reveals that the M elements were arranged at a ~120° inter-angle when viewed sinistrally. The dextral and sinistral S elements are arranged symmetrically in ventral and dorsal side views. The S_0 element is located at the middle of the S array, protruding slightly.

5.2. *Components and structure of the* Nicoraella *apparatus*

The materials viewed under SEM (Huang et al., 2019) could only show external aspects of the clusters. It is hard to discern morphology when clustered elements obscure one another and are more or less buried in associated diagenetic mineral crusts. SEM analysis alone cannot resolve the three-dimensional arrangement of elements within the clusters. However, these characters of the apparatus are resolved clearly in the SRXTM data, and enhanced through manual computed tomographic segmentation such that the elements can be discriminated in their clusters (see Figs. A1–A8 of Appendix A in Supplementary material). The element arrangement and their relative positions can also be clearly studied (Figs. 3–6).

The tomographic reconstruction shows that the clusters preserve aspects of the three-dimensionality of the feeding apparatus (Figs. 3–6), much more so than natural assemblages described previously, almost all of which are collapsed or compressed into an approximately two-dimensional plane (Purnell and Donoghue, 1998; Agematsu et al., 2014, 2017).

The clusters display consistent and repeated patterns of element juxtaposition (Figs. 2–6), and we can interpret the mor-

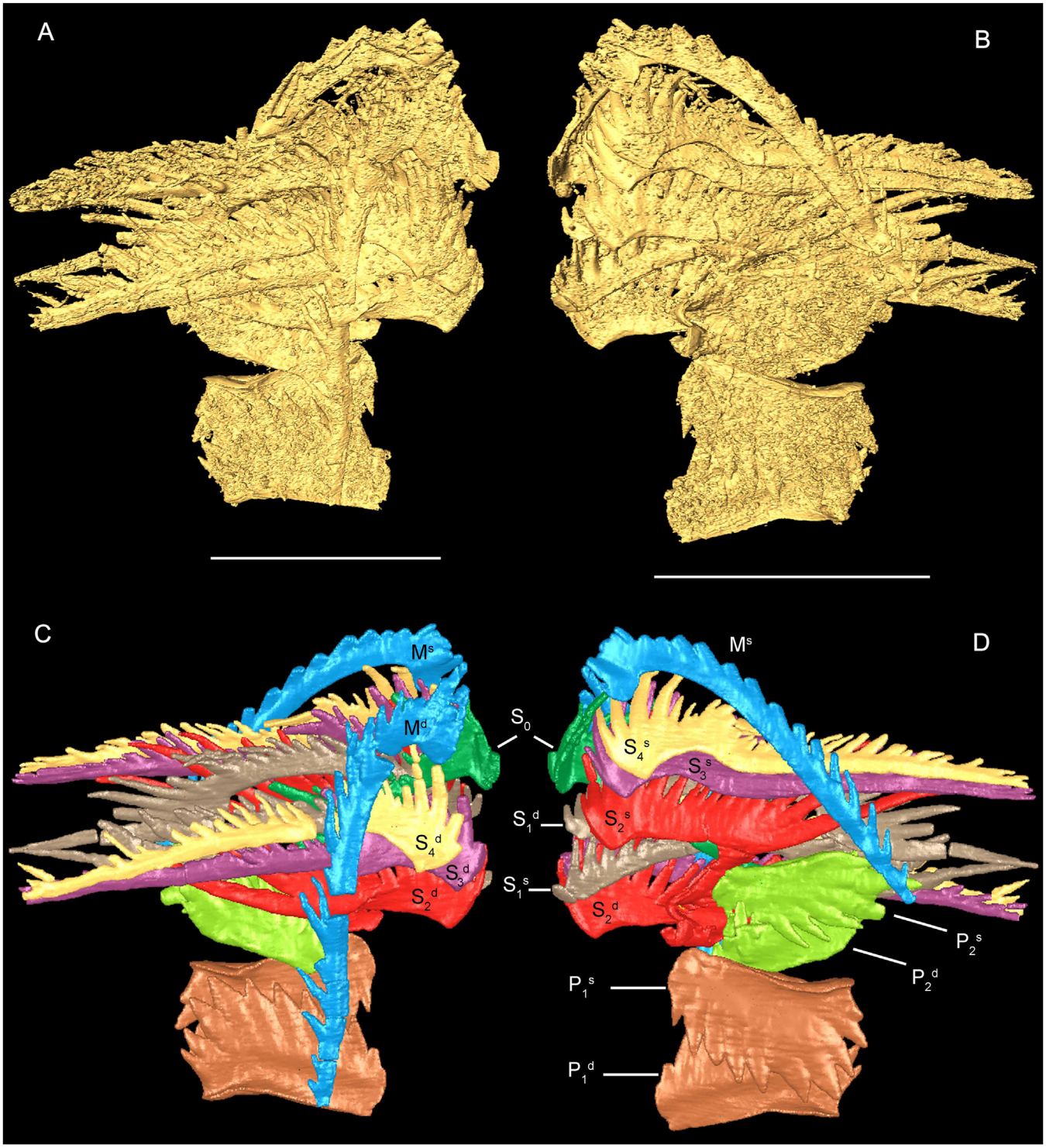

Fig. 3. Articulated conodont clusters from bed 18 in the Dawazi section (catalogue no.: pm028-18-wy1-C1). (A, B) Synchrotron images in dextral and sinistral side views. (C, D) Surface models corresponding to (A, B). Scale bar = 400 μm.

phology of each component in the apparatus in detail (Fig. 7). An alate S_0 element lies in the middle of the clusters (Figs. 2 A, 3–6), its posterior process aligned oblique to those of the other S elements, with its cusp and antero-lateral process positioned rostrad of the rest of the S elements (Fig. 6). This kind of S_0 element normally has a long posterior process and crown-shaped lateral processes, its main cusp is located at the anterior end and it is connected with two short lateral processes by a small denticle. The posterior process is slightly bent or straight in lateral view, and there is a small basal cavity among the posterior and two lateral processes (Fig. 6D).

The S domain, composed of juxtaposed ramiform elements in the S_1–S_4 and M positions, includes a bilaterally symmetrical series of breviform digyrate $S_{1–2}$ and bipennate $S_{3–4}$ elements

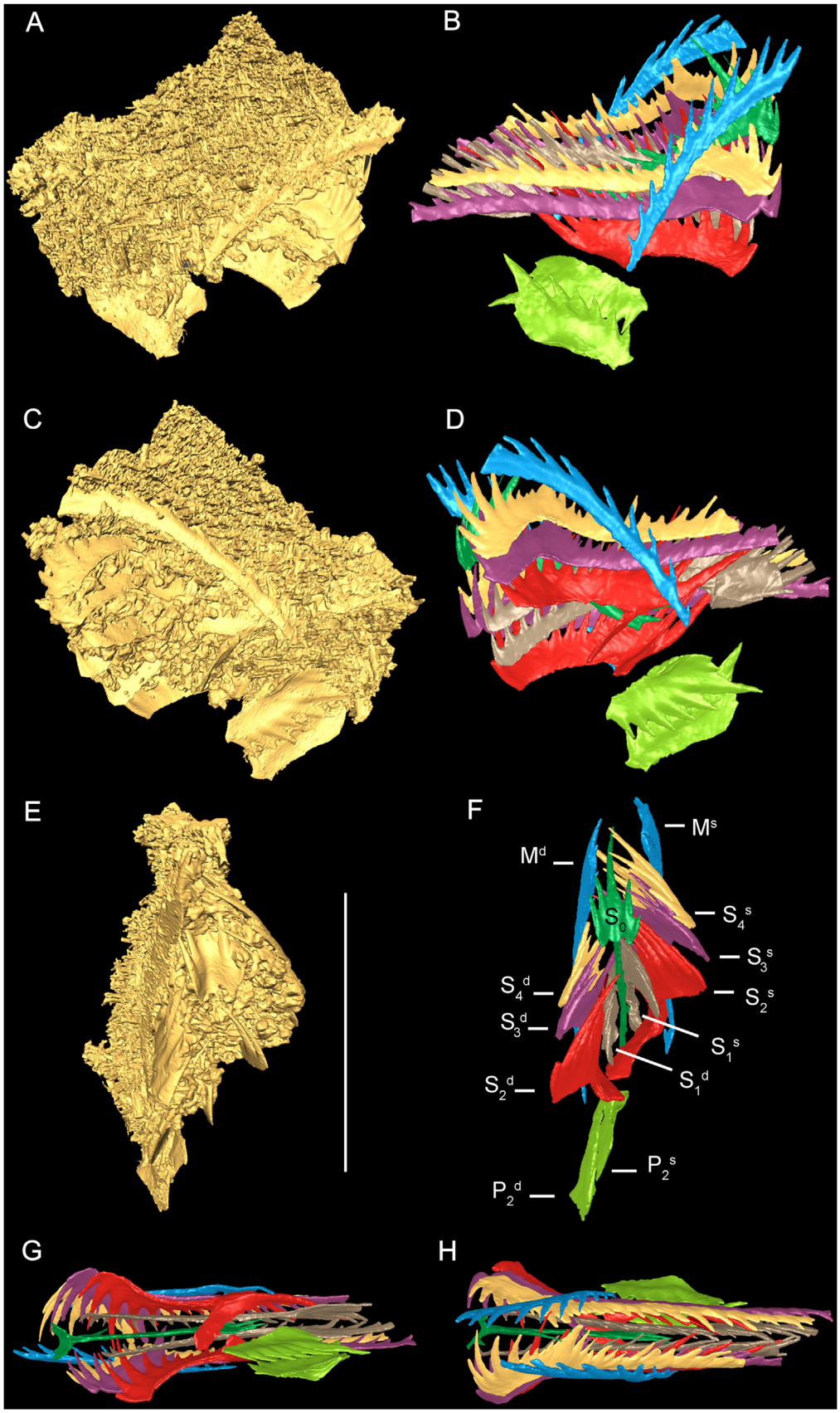

Fig. 4. Articulated conodont clusters from bed 25 in the Dawazi section (catalogue no.: pm028-25-wy1-C1). (A, C, E) Synchrotron images in the dextral, sinistral and oral side views. (B, D, F) Surface models corresponding to (A, C, E). (G, H) Surface models from the ventral and oral side views. Scale bar = 400 μm.

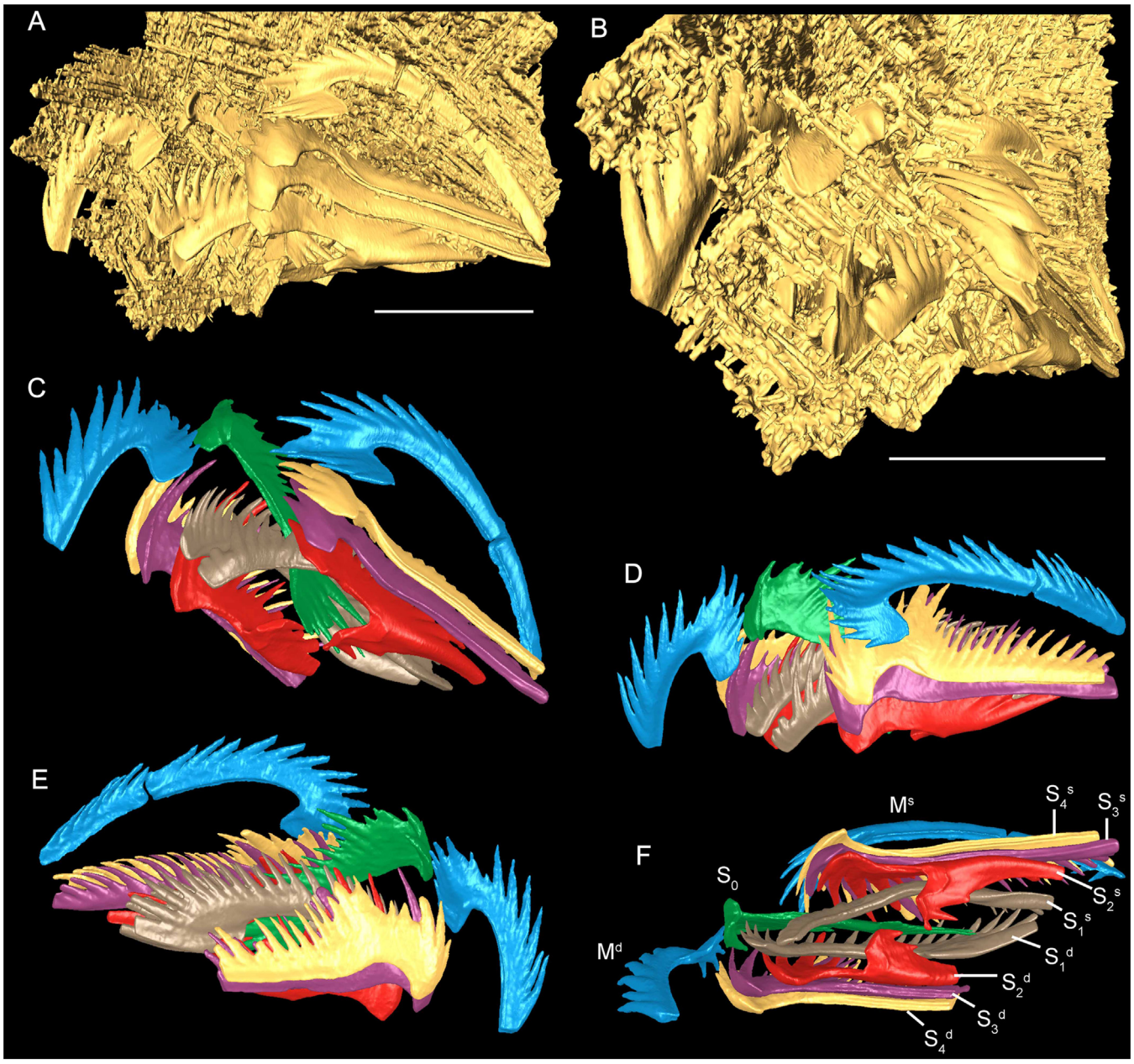

Fig. 5. Articulated conodont clusters from bed 25 in the Dawazi section (catalogue no.: pm028-25-wy1-C2). (A, B) Synchrotron images in the sinistral and oral with slightly ventral side views. (C–F) Surface models from the ventro-sinstral, sinistral, dextral and ventral side views. Scale bar = 400 μm.

from adaxial to abaxial. The S_1 elements are located on both sides of the S_0 element, and bracketed abaxially by the S_2 elements. The S_1 element has a long cusp at the end of a long anterior process, a short inner-lateral process, and the basal furrow is narrow (Fig. 4G). The prominent cusp of the S_2 element connects with a long anterior process with discrete denticles, and a shorter, slender, inner-lateral process that can also be developed and recurved. The bipennate $S_{3–4}$ elements are located abaxial to the S_2 elements, and are similar morphologically, with their cusp and denticles unfused, and the basal furrow narrow (Fig. 5C). Like the S_1 elements, the breviform digyrate M elements have a long anterior process and a robust cusp. However, the lateral process differs in possessing two to four small denticles behind the main cusp. The M elements are located abaxial of the S array.

The paired carminate P_2 elements are located between the S and P_1 elements (Fig. 3), with their anterior-posterior processes oriented approximately perpendicular to the processes of the S elements (Fig. 4D). The P_2 elements have a prominent cusp between their long anterior and short posterior process; the basal cavity is located one fourth of the way along the element, and the basal furrow is narrow. The blade-shaped P_1 elements are located caudal of the P_2 elements; the cusp lies between a well-developed anterior process and a short posterior process. The denticles are fused; the basal pit is located at one fourth of the

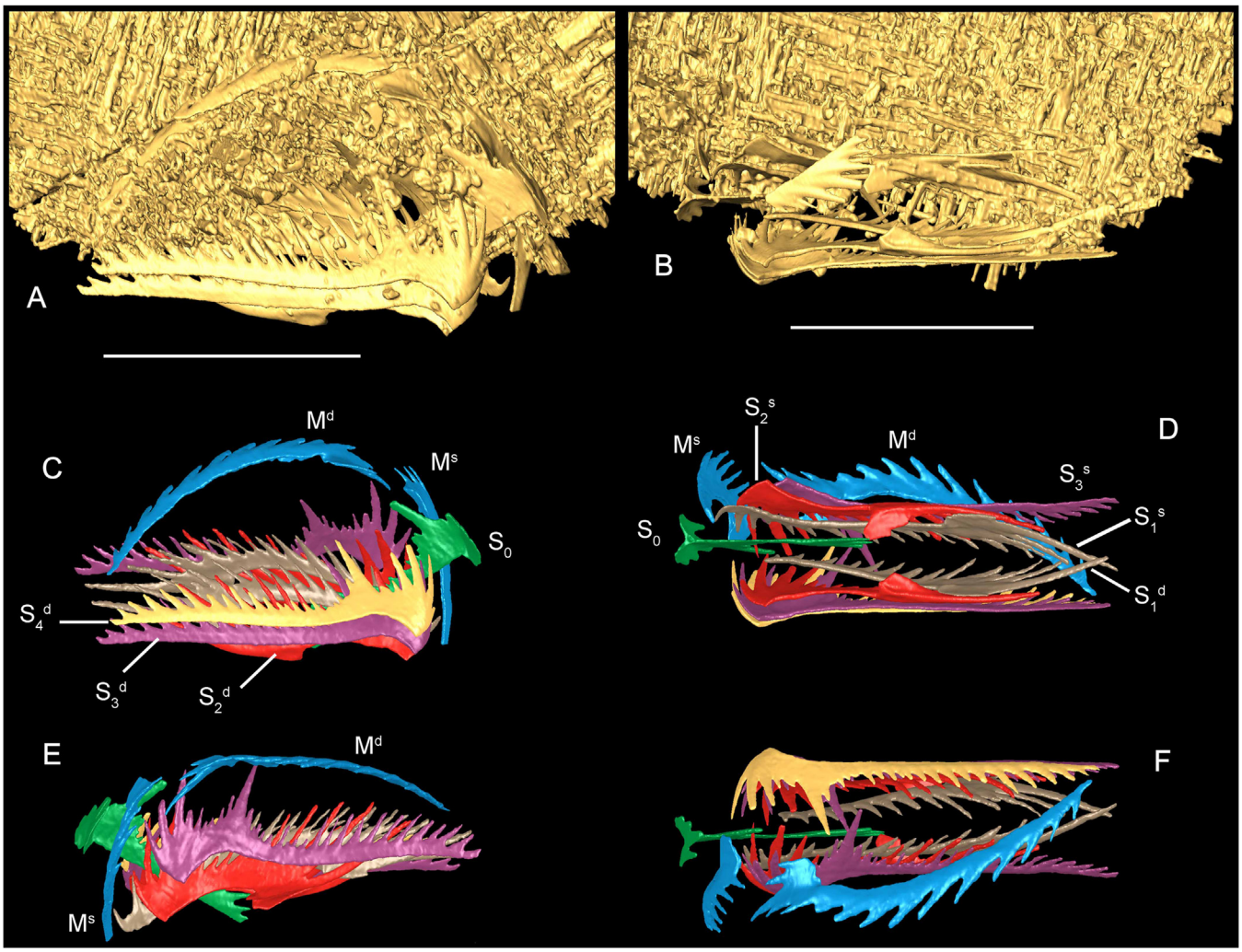

Fig. 6. Articulated conodont clusters from bed 26 in the Dawazi section (catalogue no.: pm028-26-wy1-C1). (A, B) Synchrotron images in the dextral and ventral side views. (C–F) Surface models from the dextral, ventral, sinistral and oral side views. Scale bar = 400 μm.

length of the blade, and terminally widened in aboral view. The paired P_1 and P_2 elements are oriented with opposing denticles, with the sinistral element in each pair positioned caudal to its dextral counterpart.

5.3. *Implications for the* Nicoraella *conodont apparatus*

During the last decade, synchrotron technology has been applied to solve many problems in palaeontology (Donoghue et al., 2006; Yin et al., 2015); there remains great potential for application in conodont morphology, structure, function, as well as resolution of debate over their biological affinity. Here, we confirm the composition and arrangement of elements proposed previously (Huang et al., 2019), demonstrating that the apparatus of *Nicoraella* conforms to the standard 15-element plan shared primitively among ozarkodinin, prioniodinin, and prioniodontid conodonts (9S-2M-4P; Purnell and Donoghue, 1998; Purnell et al., 2000). Aside from the P elements, the ramiform (S and M) elements are very similar in the apparatuses of the superfamily Gondolelloidea, including *Novispathodus*, *Nicoraella* and *Neogondolella*. Further, the long-term problems of element morphology and relative locations of the S_1, S_2 and P_2 positions are now clarified.

In previous reconstructions, the breviform digyrate elements of enantiognathiform and cypridodellan morphotypes were recognized as occupying the S_1 and S_2 positions, respectively (Orchard and Rieber, 1999; Kolar-Jurkovšek et al., 2005; Orchard, 2005; Sun et al., 2009), based on natural assemblages of *Neogondolella* from the Middle Triassic of Monte San Giorgio, Switzerland (Rieber, 1980). However, this assemblage is too fragmentary to assign the elements to homologous positions within the apparatus. Goudemand et al. (2011, 2012) attempted to resolve this problem based on partial clusters of *Novispathodus* and *Neogondolella* from the early Triassic of China and Switzerland. The breviform digyrate elements of cypridodellan and enantiognathiform morphotypes were identified as S_1 and S_2 elements (respectively), but the clusters lack S_0 and M elements (Goudemand et al., 2011; Fig. 2A), making it impossible to establish positional homologies. Based on our more complete clusters, we can confidently interpret the S_1 and S_2 apparatus positions to have been occupied by elements classi-

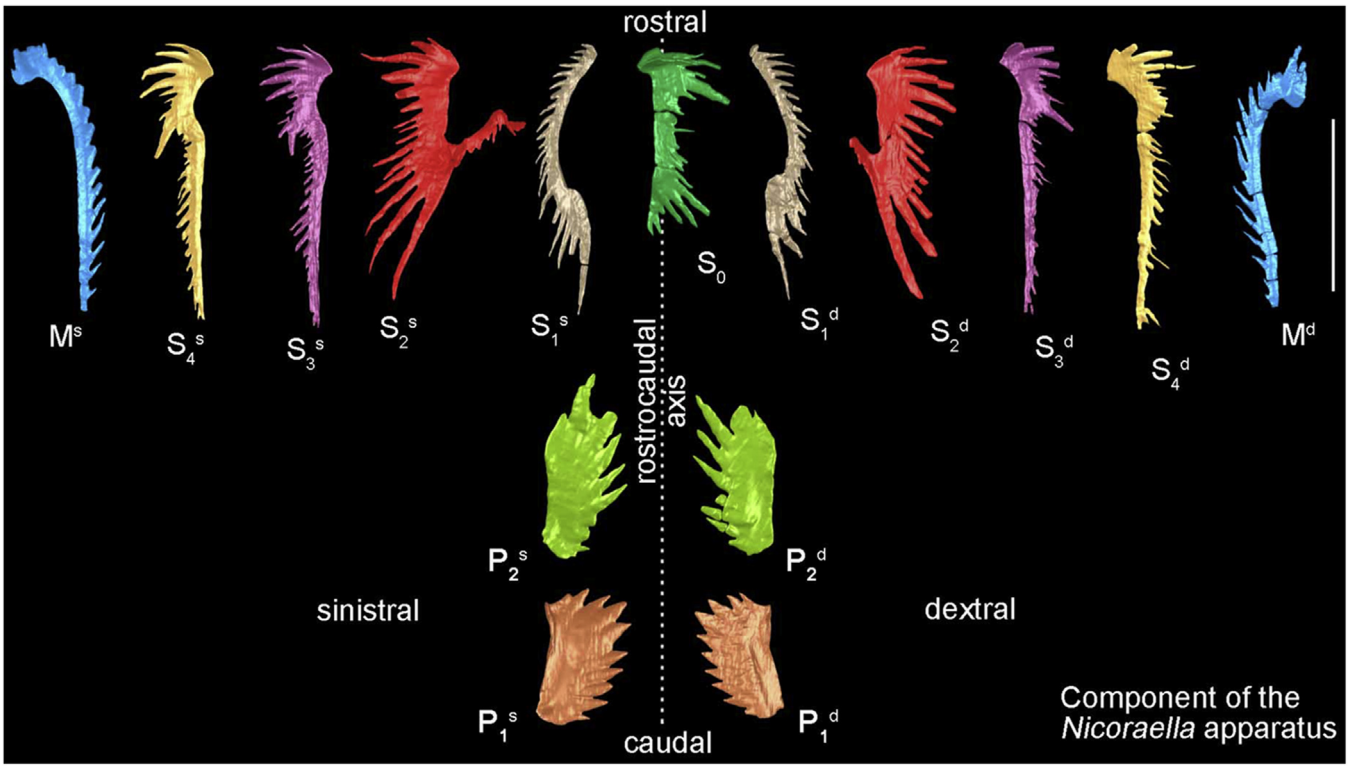

Fig. 7. Skeletal plan of *Nicoraella* apparatus based on the cluster in Fig. 3 (catalogue no.: pm028-18-wy1-C1). Topological scheme of notations is presented along with the elements respectively. Scale bar = 400 μm.

cally described as cypridodellan and enantiognathiform, as well as confirming that the elements in the S_0, $S_{3–4}$ and M positions as alate, bipennate and breviform digyrate, respectively.

The position of the P_2 element relative to the S-M array remains uncertain in *Novispathodus*. Goudemand et al. (2011) infer these element positions to have been widely spaced, as in *Idiognathodus* (Purnell and Donoghue, 1997, 1998), but there is no direct evidence for this in *Novispathodus*. If the apparatuses share a similar structure to those in the superfamily Gondolelloidea, our evidence suggests that the P_2 elements in the *Novispathodus* apparatus were located much closer to the S domain (Fig. 4B–D).

Finally, although some of our clusters appear to preserve aspects of their original three-dimensional architecture, based on SEM analysis (Huang et al., 2019), it has not previously been possible to demonstrate this directly since aspects of cluster structure are obscured by element overlap and diagenetic mineral matrix. Our use of SRXTM has allowed us to fully characterize the relative arrangement of elements within the clusters, establishing element positional homologues and, thus, apparatus composition. In future, we will advance contemporary approaches to reconstructing apparatus architecture by physical modelling (Aldridge et al., 1987, 1995, 2013; Purnell and Donoghue, 1997, 1998), through virtual modelling based on accurate tomographic characterization of the elements within natural assemblages. In this way it will be possible to constrain and test established hypotheses of conodont apparatus function and, ultimately, aid debate over the phylogenetic relationships among conodonts.

6. Conclusions

Five exceptionally fused conodont clusters are reported from the Middle Triassic strata of Member II of Guanling Formation, Dawazi section, Luoping County, Yunnan Province, Southwest China. Synchrotron microtomography has revealed the original topological homologies of elements in the apparatus of *Nicoraella*, clearly showing its element morphologies, arrangement, and number of elements in the apparatus. Accordingly, a new 15-element template is presented for *Nicoraella*, composed of a single symmetrical S_0 element, and pairs of bilaterally symmetrical S_{1-4}, M, and P_{1-2} elements, and corroborating previous studies (Huang et al., 2019). Although the new reconstructions are very similar to the apparatuses of other species within Gondolelloidea, the element morphologies occupying the S_1 and S_2 positions have been unclear. In this study, synchrotron tomographic characterization of *Nicoraella* clusters presents consistent and repeated patterns of juxtaposition, with the M element located outermost, S_0 innermost, S_4, S_3 and S_2 in a nested arrangement relative to this axial element, and the S_1 elements embraced by two short inner lateral processes of breviform digyrate S_2 elements. The S_1 and S_2 positions were occupied by cypridodellan and enantiognathiform elements, respectively. This new datum will be significant in attempts to resolve the classification and phylogeny of Gondolelloidea, allowing us to reconstruct accurately apparatus architecture and infer element functional kinematics. So far, our data represent the most complete clusters described to date, showing the composition and element arrangement in a conodont apparatus.

Data archiving statement

Three dimensional synchrotron X-ray tomographic (SRXTM) datasets and computed tomographic datasets for this study are available in repository of the Research Data Storage Facility (RDSF) of the University of Bristol. Doi: https://doi.org/10.5523/bris.yw0swm1vgiz92catj97qv8g1c, and URL links: http://data.bris.ac.uk/data/dataset/yw0swm1vgiz92catj97qv8g1c.

Acknowledgements

This work was supported from Chinese grants of the National Natural Science Foundation of China (Nos. 41502013, 41772022, 41661134047, 41572091, 41530104 and 41240016); Chinese Geological Survey projects (Nos. DD20160020 and 12120114068001); State Key Laboratory of Palaeobiology and Stratigraphy (Nanjing Institute of Geology and Palaeontology, CAS) (No. 133106); and Sylvester Bradley Award from the Palaeontological Association (UK) (No. PA-SB201401). We acknowledge further grants from the Natural Environment Research CouncilNE/G016623/1 (UK) to P.C.J. Donoghue, and Spanish Projects CGL2014-52662-P, GV/2016/102 and University of Valencia to C. Martínez-Pérez. We thank three reviewers (Dr. Yu-Ping Qi and two anonymous reviewers), and the editor for their constructive suggestions and corrections.

Appendix A. Supplementary data

Supplementary data associated with this article can be found, in the online version, at https://doi.org/10.1016/j.palwor.2018.08.003.

References

Agematsu, S., Sano, H., Sashida, K., 2014. Natural assemblages of *Hindeodus* conodonts from a Permian–Triassic boundary sequence, Japan. Palaeontology 57, 1277–1289.

Agematsu, S., Uesugi, K., Sano, H., Sashida, K., 2017. Reconstruction of the multielement apparatus of the earliest Triassic conodont, *Hindeodus parvus*, using synchrotron radiation X-ray micro-tomography. Journal of Paleontology 91, 1220–1227.

Agematsu, S., Golding, M.L., Orchard, M.J., Smith, A., 2018. Comments on: testing hypotheses of element loss and instability in the apparatus composition of complex conodonts (Zhang et al.). Palaeontology 61, 785–792.

Aldridge, R.J., Smith, M.P., Norby, R.D., Briggs, D.E.G., 1987. The architecture and function of Carboniferous polygnathacean conodont apparatuses. In: Aldridge, R.J. (Ed.), Palaeobiology of Conodonts. Ellis Horwood, Chichester, pp. 63–76.

Aldridge, R.J., Briggs, D.E.G., Smith, M.P., Clarkson, E.N.K., Clark, N.D.L., 1993. The anatomy of conodonts. Philosophical Transactions of the Royal Society of London, Series B 340, 405–421.

Aldridge, R.J., Purnell, M.A., Gabbott, S.E., Theron, J.N., 1995. The apparatus architecture and function of *Promissum pulchrum* Kovács-Endrödy (Conodonta, Upper Ordovician), and the prioniodontid plan. Philosophical Transactions of the Royal Society of London, Series B 347, 275–291.

Aldridge, R.J., Murdock, D.J.E., Gabbott, S.E., Theron, J.N., 2013. A 17-element conodont apparatus from the Soom Shale Lagerstätte (Upper Ordovician), South Africa. Palaeontology 56, 261–276.

Bai, J., Zhang, Q., Huang, J., Zhang, K., Zhou, C., Lu, T., Hu, S., 2011. Middle Triassic sequence stratigraphy and sedimentary facies analysis at the Shangshikan section of Luoping County, Yunnan Province. Journal of Stratigraphy 35, 278–287 (in Chinese, with English abstract).

Benton, M.J., Zhang, Q., Hu, S., Chen, Z., Wen, W., Liu, J., Huang, J., Zhou, C., Xie, T., Tong, J., Choo, B., 2013. Exceptional vertebrate biotas from the Triassic of China, and the expansion of marine ecosystems after the end-Permian mass extinction. Earth-Science Reviews 125, 199–243.

Chen, Y.L., Jiang, H.S., Lai, X.L., Yan, C.B., Richoz, S., Liu, X.D., Wang, L.N., 2015. Early Triassic conodonts of Jiarong, Nanpanjiang Basin, southern Guizhou Province, South China. Journal of Asian Earth Sciences 105, 104–121.

Chen, Y.L., Krystyn, L., Orchard, M.J., Lai, X.L., Richoz, S., 2016. A review of the evolution, biostratigraphy, provincialism, and diversity of Middle and early Late Triassic conodonts. Papers in Palaeontology 59, 235–263.

Chen, Z.Q., Benton, M.J., 2012. The timing and pattern of biotic recovery following the end-Permian mass extinction. Nature Geoscience 5, 375–383.

Donoghue, P.C.J., Forey, P.L., Aldridge, R.J., 2000. Conodont affinity and chordate phylogeny. Biological Reviews 75, 191–251.

Donoghue, P.C.J., Bengtson, S., Dong, X., Gostling, N.J., Huldtgren, T., Cunningham, J.A., Yin, C., Yue, Z., Peng, F., Stampanoni, M., 2006. Synchrotron X-ray tomographic microscopy of fossil embryos. Nature 442, 680–683.

Enos, P., Lehrmann, D.J., Wei, J., Yu, Y., Xiao, J., Chaikin, D.H., Minzoni, M., Berry, A.K., Miontgomery, P., 2006. Triassic Evolution of the Yangtze platform in Guizhou Province, People's Republic of China. Geological Society of America Special Paper 417, 105 pp.

Feldmann, R.M., Schweitzer, C.E., Hu, S., Zhang, Q., Zhou, C., Xie, T., Huang, J., Wen, W., 2012. Macrurous Decapoda from the Luoping Biota (Middle Triassic) of China. Journal of Paleontology 86, 425–441.

Feldmann, R.M., Schweitzer, C.E., Hu, S., Huang, J., Zhang, Q., Zhou, C., Wen, W., Xie, T., Maguire, E.P., 2017. A new Middle Triassic (Anisian) cyclidan crustacean from the Luoping Biota, Yunnan Province, China: morphologic and phylogenetic insights. Journal of Crustacean Biology 37, 406–412.

Goudemand, N., Orchard, M.J., Urdy, S., Bucher, H., Tafforeau, P., 2011. Synchrotron-aided reconstruction of the conodont feeding apparatus and implications for the mouth of the first vertebrates. Proceedings of the National Academy of Sciences, USA 108, 8720–8724.

Goudemand, N., Orchard, M.J., Tafforeau, P., Urdy, S., Brühwiler, T., Brayard, A., Galfetti, T., Bucher, H., 2012. Early Triassic conodont clusters from South China: revision of the architecture of the 15 element apparatuses of the superfamily Gondolelloidea. Palaeontology 55, 1021–1034.

Hu, S., Zhang, Q., Chen, Z.Q., Zhou, C., Lü, T., Xie, T., Wen, W., Huang, J., Benton, M.J., 2011. The Luoping biota: exceptional preservation, and new evidence on the Triassic recovery from end-Permian mass extinction. Proceedings of the Royal Society B: Biological Sciences 278, 2274–2282.

Hu, S., Zhang, Q., Feldmann, R.M., Benton, M.J., Schweitzer, C.E., Huang, J., Wen, W., Zhou, C., Xie, T., Lü, T., Hong, S., 2017. Exceptional appendage and soft-tissue preservation in a Middle Triassic horseshoe crab from SW China. Scientific Reports 7, 14112, http://dx.doi.org/10.1038/s41598-017-13319-x.

Huang, J., Zhang, K., Zhang, Q., Lü, T., Zhou, C., Bai, J., 2009. Conodonts stratigraphy and sedimentary environment of the Middle Triassic at Daaozi section of Luoping County, Yunnan Province, south China. Acta Micropalaeontologica Sinica 26, 211–224 (in Chinese, with English abstract).

Huang, J., Zhang, K., Zhang, Q., Lü, T., Hu, S., Zhou, C., 2011. Advance research of conodont fauna from Shangshikan and Daaozi sections in Luoping area, Yunnan Province. Geological Science and Technology Information 30, 1–17 (in Chinese, with English abstract).

Huang, J., Feldmann, R.M., Schweitzer, C.E., Hu, S., Zhou, C., Benton, M.J., Zhang, Q., Wen, W., Xie, T., 2013. A new shrimp (Decapoda, Dendrobranchiata, Penaeoidea) from the Middle Triassic of Yunnan, Southwest China. Journal of Paleontology 87, 603–611.

Huang, J., Hu, S., Zhang, Q., Donoghue, P.C.J., Benton, M.J., Zhou, C., Martinez-Perez, C., Wen, W., Xie, T., Chen, Z.Q., Luo, M., Yao, H., Zhang, K., 2019. Gondolelloid multielement conodont apparatus (*Nicoraella*) from the Middle Triassic of Yunnan Province, southwestern China. Palaeogeography, Palaeoclimatology, Palaeoecology 522, 98–110.

Jiang, H., Luo, G., Lai, X., 2004. Summary of approaches for conodont separation. Geological Science and Technology Information 23, 109–112 (in Chinese, with English abstract).

Jiang, H., Lai, X., Luo, G., Aldridge, R., Zhang, K., Wignall, P., 2007. Restudy of conodont zonation and evolution across the P/T boundary at Meishan section, Changxing, Zhejiang, China. Global and Planetary Change 55, 39–55.

Jiang, H., Lai, X., Yan, C., Aldridge, R.J., Wignall, P., Sun, Y., 2011. Revised conodont zonation and conodont evolution across the Permian–Triassic boundary at the Shangsi section, Guangyuan, Sichuan, South China. Global and Planetary Change 77, 103–115.

Joachimski, M.M., Lai, X., Shen, S., Jiang, H., Luo, G., Chen, B., Chen, J., Sun, Y., 2012. Climate warming in the latest Permian and the Permian–Triassic mass extinction. Geology 40, 195–198.

Jones, D.O., Evans, A.R., Rayfield, E.J., Siu, K.K., Donoghue, P.C.J., 2012a. Testing micro structural adaptation in the earliest dental tools. Biology Letters 8, 952–955.

Jones, D.O., Evans, A.R., Rayfield, E.J., Siu, K.K., Donoghue, P.C.J., 2012b. The sharpest tools in the box? Quantitative analysis of conodont element functional morphology. Proceedings of the Royal Society B: Biological Sciences 279, 2849–2854.

Kolar-Jurkovšek, T., Gaździcki, A., Jurkovšek, B., 2005. Conodonts and foraminifera from the "Raibl Beds" (Carnian) of the Karavanke Mountains, Slovenia: stratigraphical and palaeobiological implications. Geological Quarterly 49, 429–438.

Liu, J., Organ, C.L., Benton, M.J., Brandley, M.C., Aitchison, J.C., 2017. Live birth in an archosauromorph reptile. Nature Communications 8, 14445, http://dx.doi.org/10.1038/ncomms14445.

Luo, M., Hu, S., Benton, M.J., Shi, G.R., Zhao, L., Huang, J., Song, H., Wen, W., Zhang, Q., Fang, Y., Huang, Y., Chen, Z.Q., 2017. Taphonomy and palaeobiology of early Middle Triassic coprolites from the Luoping biota southwest China: implications for reconstruction of fossil food webs. Palaeogeography, Palaeoclimatology, Palaeoecology 474, 232–246.

Luo, M., Shi, G.R., Hu, S., Benton, M.J., Chen, Z.Q., Huang, J., Zhang, Q., Zhou, C., Wen, W., 2019. Early Middle Triassic trace fossils from the Luoping Biota, southwestern China: Evidence of recovery from mass extinction. Palaeogeography, Palaeoclimatology, Palaeoecology 515, 6–22.

Marone, F., Münch, B., Stampanoni, M., 2010. Fast reconstruction algorithm dealing with tomography artifacts. Proceedings of SPIE 7804, 780410, http://dx.doi.org/10.1117/12.859703.

Martínez-Pérez, C., Rayfield, E.J., Purnell, M.A., Donoghue, P.C.J., 2014a. Finite element, occlusal, microwear and microstructural analyses indicate that conodont microstructure is adapted to dental function. Palaeontology 57, 1059–1066.

Martínez-Pérez, C., Plasencia, P., Jones, D., Kolar-Jurkovšek, T., Sha, J., Botella, H., Donoghue, P.C.J., 2014b. There is no general model for occlusal kinematics in conodonts. Lethaia 47, 547–555.

Martínez-Pérez, C., Rayfield, E.J., Botella, H., Donoghue, P.C.J., 2016. Translating taxonomy into the evolution of conodont feeding ecology. Geology 44, 247–250.

Mazza, M., Martínez-Pérez, C., 2015. Unravelling conodont (Conodonta) ontogenetic processes in the Late Triassic through growth series reconstructions and X-ray microtomography. Bollettino della Società Paleontologica Italiana 54, 161–186.

Mazza, M., Martínez-Pérez, C., 2016. Evolutionary convergence in conodonts revealed by Synchrotron-based Tomographic Microscopy. Palaeontologia Electronica 19 (3), 52A, http://dx.doi.org/10.26879/681.

Murdock, D.J.E., Sansom, I.J., Donoghue, P.C.J., 2013a. Cutting the first 'teeth' — a new approach to functional analysis of conodont elements. Proceedings of the Royal Society B: Biological Sciences 280, 20131524.

Murdock, D.J.E., Dong, X.P., Repetski, J.E., Marone, F., Stampanoni, F.M., Donoghue, P.C.J., 2013b. The origin of conodonts and of vertebrate mineralized skeletons. Nature 502, 546–549.

Murdock, D.J.E., Rayfield, E.J., Donoghue, P.C.J., 2014. Functional adaptation underpinned the evolutionary assembly of the earliest vertebrate skeleton. Evolution & Development 16, 354–361.

Orchard, M.J., 2005. Multielement conodont apparatuses of Triassic Gondolelloidea. Special Papers in Palaeontology Series 73, 73–101.

Orchard, M.J., Rieber, H., 1999. Multielement *Neogondolella* (Conodonta, upper Permian–middle Triassic). Bollettino della Società Paleontologica Italiana 37, 475–488.

Purnell, M.A., Donoghue, P.C.J., 1997. Architecture and functional morphology of the skeletal apparatus of ozarkodinid conodonts. Philosophical Transactions of the Royal Society of London, Series B 352, 1545–1564.

Purnell, M.A., Donoghue, P.C.J., 1998. Skeletal architecture, homologies and taphonomy of ozarkodinid conodonts. Palaeontology 41, 57–102.

Purnell, M.A., Donoghue, P.C.J., Aldridge, R.J., 2000. Orientation and anatomical notation in conodonts. Journal of Paleontology 74, 113–122.

Purnell, M.A., Zhang, M., Jiang, H., Lai, X., 2018. Reconstruction, composition and homology of conodont skeletons: a response to Agematsu et al. Palaeontology 61, 793–796.

Rieber, H., 1980. Ein Conodonten-cluster aus der Grenzbitumenzone (Mittlere Trias) des Monte San Giorgio (Kt. Tessin/Schweiz). Annalen des Naturhistorischen Museums in Wien 83, 265–274.

Sun, Y.D., Joachimski, M., Wignall, P.B., Yan, C.B., Chen, Y.L., Jiang, H.S., Wang, L.N., Lai, X.L., 2012. Lethally hot temperatures during the Early Triassic greenhouse. Science 338, 366–370.

Sun, Z., Hao, W., Sun, Y., Jiang, D., 2009. The conodont genus *Nicoraella* and a new species from the Anisian of Guizhou South China. Neues Jahrbuch für Geologie und Paläontologie, Abhandlungen 252, 227–235.

Suttner, T.J., Kido, E., Briguglio, A., 2017. A new icriodontid conodont cluster with specific mesowear supports an alternative apparatus motion model for Icriodontidae. Journal of Systematic Palaeontology 16, 909–926.

Wen, W., Zhang, Q., Hu, S., Zhou, C., Xie, T., Huang, J., Chen, Z.Q., Benton, M.J., 2012. A new genus of basal actinopterygian fish from the Anisian (Middle Triassic) of Luoping, Yunnan Province, Southwest China. Acta Palaeontologica Polonica 57, 149–160.

Wen, W., Zhang, Q., Hu, S., Benton, M.J., Zhou, C., Tao, X., Huang, J., Chen, Z.Q., 2013. Coelacanths from the Middle Triassic Luoping Biota, Yunnan, South China, with the earliest evidence of ovoviviparity. Acta Palaeontologica Polonica 58, 175–193.

Yin, Z., Zhu, M., Davidson, E.H., Bottjer, D.J., Zhao, F., Tafforeau, P., 2015. Sponge grade body fossil with cellular resolution dating 60 Myr before the Cambrian. Proceedings of the National Academy of Sciences, USA 112, E1453–E1460.

Zhang, M., Jiang, H., Purnell, M.A., Lai, X., 2017. Testing hypotheses of element loss and instability in the apparatus composition of complex conodonts: articulated skeletons of *Hindeodus*. Palaeontology 60, 595–608.

Zhang, Q., Zhou, C., Lü, T., Xie, T., Lou, X., Liu, W., Sun, Y., Huang, J., Zhao, L., 2009. A conodont-based Middle Triassic age assignment for the Luoping Biota of Yunnan, China. Science in China Series D: Earth Sciences 52, 1673–1678.